

Simulating a two-dimensional frustrated spin system with fermionic resonating-valence-bond states

Chung-Pin Chou¹ and Hong-Yi Chen²

¹Beijing Computational Science Research Center, Beijing 100084, China and
²Department of Physics, National Taiwan Normal University, Taipei 116, Taiwan

The frustrated Heisenberg $J_1 - J_2$ model on a square lattice is numerically investigated by variational Monte Carlo simulations. We propose a antiferromagnetic fermion resonating-valence-bond (AF-fRVB) state that has ability to examine the entire phase diagram in the $J_1 - J_2$ model. Two phase transition points, the second order around $J_2/J_1 = 0.45$ and the first order around $J_2/J_1 = 0.6$, can be extracted more clearly than the conventional bosonic RVB state. At the maximally frustrated point ($J_2/J_1 = 0.5$), the AF-fRVB state shows the variational ground-state energy in the thermodynamic limit very close to the one estimated by the projected entangled pair state at the largest bond dimension available. On the other hand, in the frustrated regime $0.4 \lesssim J_2/J_1 \leq 0.5$, AF-fRVB states with s_{+-} (using the terminology in the field of iron-based superconductors) and d_{xy} pairing symmetries are degenerate in the thermodynamic limit, implying the existence of gapless Dirac excitations in the spinon spectrum.

PACS numbers: 75.10.Kt, 75.10.Jm, 71.10.Hf

Introduction. Frustration is one of the simplest concepts to induce a quantum phase transition in magnetic systems. Quantum spin liquids, searched for both theoretically and experimentally over decades, could be one of the products in frustrated spin models^{1,2}. Notably, studies of quantum phase transitions between spin-liquid phases and adjacent magnetically ordered phases are important to understand quantum spin liquids. To tackle the problem about the quantum phase transition, a systematic analysis of the detailed ground-state phase diagram of frustrated spin systems is required. The zero-temperature phase diagram of the spin-1/2 $J_1 - J_2$ square lattice model has been reported by exact diagonalization (ED) calculations^{3,4} and large-scale density matrix renormalization group (DMRG) studies^{5,6}. It is well known that the ground state displays a checkerboard antiferromagnetic (AF) order at small J_2/J_1 and a collinear AF order at large J_2/J_1 . However, the existence of a gapless or gapful quantum spin liquid between checkerboard and collinear AF ordered phases has still remained unsolved.

To date, most of variational Monte Carlo (VMC) studies of the $J_1 - J_2$ model mainly focus on the maximally frustrated regime ($J_2/J_1 \sim 0.5$) and search a possible quantum spin liquid by using either Schwinger bosonic or fermionic resonating-valence-bond (RVB) wave functions⁷⁻¹³. The RVB theory is the first proposal by Anderson to describe the quantum spin liquid in a two-dimensional (2D) spin-1/2 Heisenberg model¹⁴. Aftermentioned, the bosonic RVB wave function, categorized by the projective symmetry group¹⁵, has been widely used to study different spin models¹⁶⁻¹⁸. On the other hand, the fermionic RVB wave function, constructed by the Gutzwiller projection onto BCS mean-field states, has predicted the existence of a gapless spin liquid in several different lattice structures¹⁹⁻²¹. However, both bosonic and fermionic RVB states fail to demonstrate the quantum phase transition involving the long-range magnetic order.

Recently, a tremendous numerical effort using the projected entangled pair states (PEPS) has been performed. The numerical result shows some missing data in a large part of the collinear regime²². It can be expected that when the ground state is on the verge of various instabilities around

critical points²³, it is very difficult to distinguish the PEPS with similar energies but different physical properties. On the other hand, since the Gutzwiller projection enables the ground state to recover symmetries lost in the BCS Hamiltonian, a Gutzwiller-projected BCS wave function is invariant with respect to the $SU(2)$ transformation implying high degeneracies after the projection. An ideal Gutzwiller-projected wave function for the 2D frustrated Heisenberg model can be thus obtained by using gap functions with different pairing symmetries²⁴.

In this work, we simply extend the Gutzwiller-projected BCS wave function to construct the fermionic RVB state which has explicit AF magnetic orders, e.g. checkerboard or collinear long-range patterns. We call it the AF fermion RVB (AF-fRVB) state. The variational framework can demonstrate the phase transition between the magnetic order and quantum spin disorder. Thus, this idea allows us to determine the ground-state phase diagram of the $J_1 - J_2$ model by using the VMC technique. Our main findings are the following: (1) the zero-temperature phase diagram is successfully reproduced by the AF-fRVB wave function; (2) a continuous phase transition near $J_2/J_1 \sim 0.45$ and clear first-order phase transition at $J_2/J_1 = 0.6$ are numerically confirmed; (3) a much less computational cost in the AF-fRVB wave function than the PEPS is performed. In particular, at $J_2/J_1 = 0.5$, the best energy obtained from the AF-fRVB state is very close to the one reached by the PEPS with rather large bond dimension; (4) in the highly frustrated regime, the next-nearest-neighbor pairing symmetry of the AF-fRVB state can be either d_{xy} or s^{+-} . The $SU(2)$ symmetry suggests that the BCS Hamiltonian with Dirac nodes reflects the gapless nature of the physical excitation spectrum.

Numerical Method. We begin with the Hamiltonian,

$$H = J_1 \sum_{\langle i,j \rangle} \mathbf{S}_i \cdot \mathbf{S}_j + J_2 \sum_{\ll i,j \gg} \mathbf{S}_i \cdot \mathbf{S}_j, \quad (1)$$

where $\langle i, j \rangle$ and $\ll i, j \gg$ denote nearest and next-nearest neighbors, respectively. \mathbf{S}_i is the spin operator at site i , and $J_1 \equiv 1, J_2 > 0$. We consider the $L \times L$ square lattice with periodic boundary condition of size $L = 8, 16, 20, 24$. The AF-

fRVB wave function we used here is based on the fermionic projective ansatz. The Gutzwiller-projected wave function in the $J_1 - J_2$ model for $0 \leq J_2 \leq 1$ is given by

$$|\Psi_{AF-fRVB}\rangle = \hat{P}_J \hat{P}_G |\Psi_0\rangle, \quad (2)$$

where $\hat{P}_G \equiv \prod_i (1 - \hat{n}_{i\uparrow} \hat{n}_{i\downarrow})$ and \hat{P}_J is the spin-spin Jastrow correlator. $\hat{n}_{i\sigma} = c_{i\sigma}^\dagger c_{i\sigma}$ is the local density. The mean-field wave function $|\Psi_0\rangle$ is constructed by diagonalizing the mean-field Hamiltonian,

$$H_{MF} = - \sum_{\langle i,j \rangle, \sigma} t_{ij} c_{i\sigma}^\dagger c_{j\sigma} + \sum_{i,j} \Delta_{ij} c_{i\uparrow}^\dagger c_{i\downarrow}^\dagger + H.c. \\ + \sum_{i,\sigma} \sigma m_i c_{i\sigma}^\dagger c_{i\sigma}. \quad (3)$$

Here we only consider the nearest neighbor hopping and $t_{ij} \equiv 1$. The real pairing amplitude Δ_{ij} is taken as the nearest neighbor (Δ_1) term and the next nearest neighbor (Δ_2) term. They can have different values along directions mutually perpendicular, e.g. $\Delta_{1,x}$, $\Delta_{1,y}$ and $\Delta_{2,x+y}$, $\Delta_{2,x-y}$.

Based on the pairing symmetry, the projected state with the constraint of one fermion per site can describe different spin liquids with the gapped or gapless spinon spectrum¹⁵. Depending on the sign structure of Δ_1 and Δ_2 along both perpendicular directions, we can have different pairing symmetries for Δ_1 and Δ_2 : (1) $d_{x^2-y^2}$ ($\Delta_{1,x}\Delta_{1,y} < 0$) and s^{++} ($\Delta_{1,x}\Delta_{1,y} > 0$) for Δ_1 ; (2) d_{xy} ($\Delta_{2,x+y}\Delta_{2,x-y} < 0$) and s^{+-} ($\Delta_{2,x+y}\Delta_{2,x-y} > 0$) for Δ_2 . Notations of s^{++} and s^{+-} are often used in the field of iron-based superconductors²⁵. The AF order parameter m_i can have two spatial patterns: checkerboard ($J_2 = 0$) or collinear ($J_2 = 1$). Once the pattern is given, the amplitude of the order parameter would be homogeneous at each site, namely, $|m_i| \equiv m$. The variational degree of freedom from the AF order can help capture the exact phase diagram in contrast to the simple fermionic RVB states.

The spin-spin Jastrow correlator \hat{P}_J is defined as

$$e^{\sum_{i<j} \kappa_{ij} \hat{S}_i^z \hat{S}_j^z}, \quad (4)$$

where $\kappa_{ij} \equiv \ln(r_{ij}^\beta w_\gamma^{\delta_{j,i+\gamma}})$. Here r_{ij} is the chord length of $|\vec{r}_i - \vec{r}_j|$ and \hat{S}_i^z is the spin operator along the z -direction at site i . In addition to the parameter β controlling long-range spin correlations, we further consider the other three parameters w_γ for the nearest ($\gamma = 1$), second-nearest ($\gamma = 2$) and third-nearest ($\gamma = 3$) neighbor spin-spin correlation. The Jastrow correlator \hat{P}_J can describe the ferromagnetic (antiferromagnetic) correlation if $S_i^z S_j^z > 0$ (< 0). In the case of $w_\gamma < 1$, for example, the short-range ferromagnetic (antiferromagnetic) correlation would be suppressed (enhanced). On the other hand, the factor r_{ij}^β controls the short-range ($r_{ij} < 1$) and long-range ($r_{ij} > 1$) correlation in an opposite way. In the long-range case, for instance, it would decrease (increase) ferromagnetic (antiferromagnetic) correlation if $\beta < 0$. In the following, we would illustrate that only seven variational parameters are needed to optimize energy, which are $\Delta, \Delta', m, w_{\gamma=1,2,3}, \beta$, and almost reach the

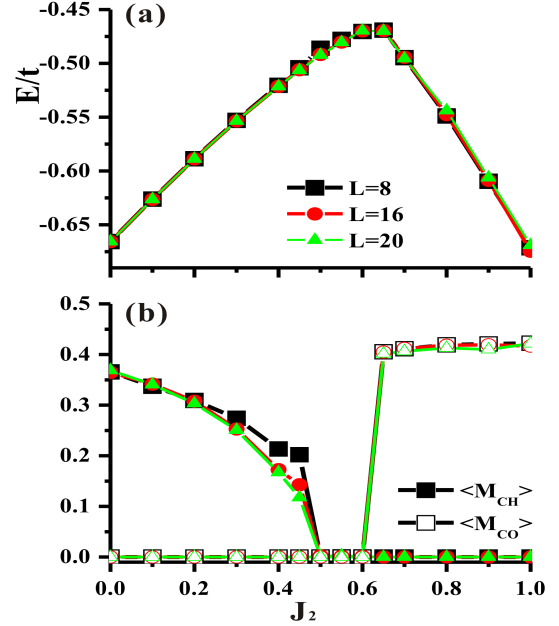


FIG. 1: (a) The optimized energy per site of the AF-fRVB states on the lattice with $N = L \times L$ sites versus J_2 . (b) The variational phase diagram for the $J_1 - J_2$ model on the square lattice. Filled (Empty) symbols represent the checkerboard (collinear) AF magnetization ($\langle M_{CH} \rangle$) ($\langle M_{CO} \rangle$). Different colors denote different lattice size as shown in (a).

same energy as the tensor-network state with a large number of variational parameters.

Results. Fig. 1(a) reveals the optimized energy of the AF-fRVB state with both RVB correlations and magnetic orders. The fermionic ansatz for the ground-state wave function including the RVB pairing and the long-range AF order successfully reproduces the frustration-induced maximum of the ground-state energy versus J_2 obtained by several ED results^{4,26,27}. The optimized energy shows much weaker size dependence than the magnetization in the intermediate regime ($0.3 \leq J_2 \leq 0.5$), as shown in Fig.1(b). For two extreme cases: $J_2 \sim 0$ and $J_2 \sim 1$, the AF-fRVB wave function can approach the AF state associated with the checkerboard or collinear pattern.

Two interesting phenomena should be emphasized. First, the finite size calculation shows that the checkerboard AF phase would survive from $J_2 = 0$ to 0.5. At a first glance this result seems to be inconsistent with the ground-state phase diagram obtained by ED and DMRG. However, in the regime of $0.3 \leq J_2 \leq 0.5$ the magnetization $\langle M_{CH} \rangle$ is obviously reduced by increasing the size of a lattice. It is necessary to conclude the position of the transition point by further examining the larger lattice size. In addition, the collinear AF phase suddenly appears at $J_2 = 0.6$, implying a possible first-order transition. Secondly, the AF-fRVB wave function would go back to the fermionic RVB state without any magnetic order in the highly frustrated regime, $0.5 < J_2 < 0.6$, which displays the typical behavior of the quantum spin liquid.

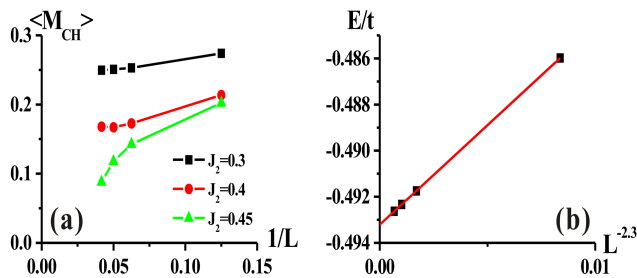


FIG. 2: Finite-size scaling of (a) the checkerboard AF magnetization $\langle M_{CH} \rangle$ for different J_2 and (b) the variational ground-state energy at $J_2 = 0.5$.

In order to examine the phase transition point, we calculate the finite size scaling of the magnetization. In Fig.2(a), it is obvious that the checkerboard AF magnetization $\langle M_{CH} \rangle$ approaches zero at $J_2 = 0.45$ in the thermodynamic limit, in contrast to cases of $J_2 = 0.3$ and 0.4 . Thus the transition point between the checkerboard AF state and the spin liquid can be clearly estimated around $J_2 = 0.45$ which is closer to recent DMRG results⁶. On the other hand, at the strongest frustration point ($J_2 = 0.5$), Fig.2(b) shows that the ground-state energy per site is extrapolated to $-0.4932(1)$ by using size scaling with the finite exponent, -2.3 . The ground-state energy of the AF-fRVB state only with seven parameters is very close to $-0.4943(7)$ obtained by the PEPS with rather large bond dimension in the thermodynamic limit²², and also much lower than $-0.4893(2)$ acquired by the Schwinger bosonic RVB wave function¹³. Moreover, the AF-fRVB wave function on a 16×16 lattice system surprisingly shows much lower optimized energy ($-0.4917(4)$) at $J_2 = 0.5$ than other tensor network states, such as the entangled-plaquette state ($-0.46299(3)$)⁹ and the renormalized tensor product state (-0.45062)²⁸. Therefore, the fermionic ansatz for the ground state of the $J_1 - J_2$ model not only reproduces the whole phase diagram but also obtains a reasonable energy to further understand the behavior of the quantum spin liquid in the intermediate regime.

As pointed out in Ref. 10, they compute the static spin structure factor to demonstrate that a fully gapped bosonic RVB state can capture the critical points of the $J_1 - J_2$ model in which the spin liquid is connected to the checkerboard AF phase through a continuous transition at $J_2 = 0.4$ and to the collinear AF state through a first-order transition at $J_2 = 0.6$. Here we emphasize that the AF-fRVB state can easily reach qualitatively similar conclusion as the bosonic RVB state, but is much more accurate than the bosonic one near the magnetically ordered regime. In Fig.3(a), either the nearest-neighbor energy (E_{J_1}) or the next-nearest-neighbor energy (E_{J_2}) continuously changes around $J_2 = 0.45$ where the checkerboard AF magnetization $\langle M_{CH} \rangle$ drops down to zero, thus exhibiting a second-order transition to the spin liquid at $J_2 = 0.45$. However, the energy encounter a sudden jump when the collinear AF phase appears at $J_2 = 0.6$, which obviously indicates a first-order phase transition.

On the other hand, variational parameters about the pair-

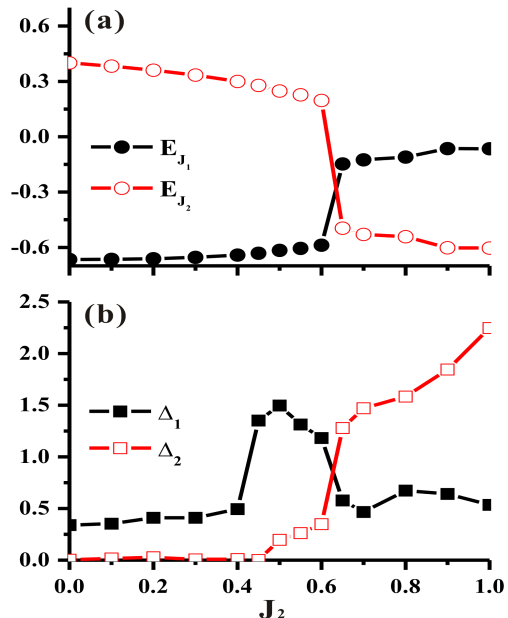


FIG. 3: (a) The nearest-neighbor energy E_{J_1} and the next-nearest-neighbor energy E_{J_2} in the $J_1 - J_2$ model as a function of J_2 . (b) The optimized parameter for the nearest-neighbor pairing Δ_1 and the next-nearest-neighbor pairing Δ_2 of the AF-fRVB state vs J_2 . The size of the lattice is 20×20 .

ing of the AF-fRVB state also display the peculiar behavior as these magnetic phases are transitioned to the spin-liquid state. In Fig.3(b), we show that the pairing parameter Δ_2 with d_{xy} symmetry is nonzero in the regime $J_2 \gtrsim 0.45$ and rapidly increased beyond $J_2 = 0.6$. More explicitly, the nonvanishing Δ_2 of the AF-fRVB wave function breaks the $U(1)$ gauge symmetry, and makes the Z_2 symmetry for the quantum spin liquid. Furthermore, the pairing Δ_1 with $d_{x^2-y^2}$ symmetry shows a bump in the spin-liquid regime ($0.45 \leq J_2 \leq 0.6$) which would favor to stabilize the spin-liquid phase. Together with the vanishing magnetization, therefore, these two optimized pairings Δ_1 and Δ_2 of the AF-fRVB state give evidence for the existence of quantum spin liquid in the frustrated regime of the $J_1 - J_2$ model.

In order to investigate possible pairing symmetries in the spin-liquid phase of the frustrated model, we also consider different pairing structures of the AF-fRVB state. Due to the pattern of the local Hamiltonian, we examine both $s_{++}/d_{x^2-y^2}$ symmetry for the nearest-neighbor pairing Δ_1 and s_{+-}/d_{xy} for the next-nearest-neighbor Δ_2 . It is worth pointing out that the variational energy cannot be optimized if we consider s_{++} symmetry in Δ_1 (not shown). The reason is that the $d_{x^2-y^2}$ singlet pair would avoid the on-site Coulomb repulsion so that the $d_{x^2-y^2}$ symmetry is more favorable than s_{++} in the Heisenberg model²⁹. As for Δ_2 , interestingly, the s_{+-} symmetry always competes with the d_{xy} symmetry for $J_2 \leq 0.4$ as shown in Fig.4(a).

In the intermediate regime ($0.4 < J_2 \leq 0.5$), nevertheless, the AF-fRVB wave function with s_{+-} symmetry shows much

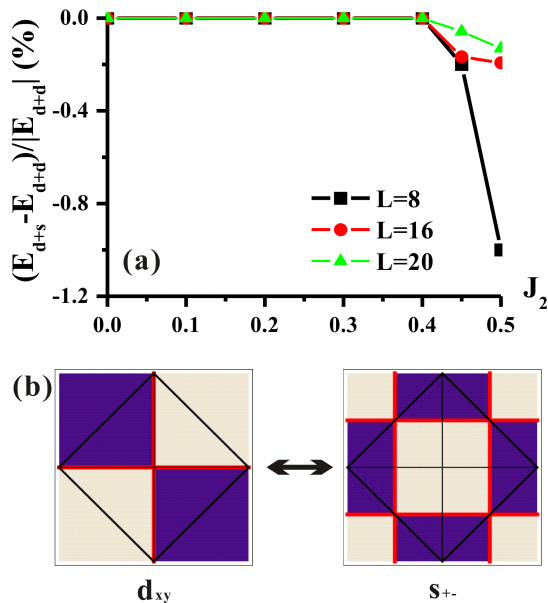


FIG. 4: (a) The percentage of the energy difference between $d_{x^2-y^2} + d_{xy}$ ($d+d$) and $d_{x^2-y^2} + s_{+-}$ ($d+s$) AF-fRVB states as a function of J_2 for different lattice size. (b) d_{xy} and s_{+-} pairing structures plotted in the first Brillouin zone. The black diamond is the spinon Fermi surface. White (Blue) regions present the positive (negative) pairing gap. Red lines mean the nodal line.

lower energy than the one with d_{xy} symmetry in finite-size calculations. Notably, a further finite-size analysis illustrates that the energy difference becomes smaller as increasing the size of lattice. Thus it is reasonable to infer that the AF-fRVB wave functions with s_{+-} and d_{xy} symmetry are always degenerate in the thermodynamic limit. Since Fig.2(a) shows that there is no long-range magnetic order ($m_i = 0$) in the intermediate regime ($0.4 < J_2 \leq 0.5$), Eq.(3) is just the mean-field BCS Hamiltonian that can be easily diagonalized,

$$E_k = \sqrt{\varepsilon_k^2 + \Delta_k^2}, \quad (5)$$

where $\varepsilon_k = -2(\cos(k_x) + \cos(k_y))$ and Δ_k is the gap function consisting of both the nearest-neighbor pairing Δ_1 and the next-nearest-neighbor pairing Δ_2 . According to the spinon spectrum E_k , the degeneracy can be understood by their equivalent nodal structures if we simply shift the spinon Fermi surface (black diamond, $\varepsilon_k = 0$) by (π, π) shown in Fig.4(b). Note that plus the $d_{x^2-y^2}$ -wave form factor, the energy dispersion E_k with both $d_{x^2-y^2}$ and s_{+-} pairing symmetries ($d+s$) clearly displays four nodes at $(\pm\pi/2, \pm\pi/2)$. Therefore, the spin-liquid state should be gapless because of the mean-field spinon spectrum with four Dirac points at $(\pm\pi/2, \pm\pi/2)$ for the $d+s$ pairing structure.

Conclusions. We have numerically studied the ground-state phase diagram of the $J_1 - J_2$ Heisenberg model on a square lattice based on the AF-fRVB wave function. The fermionic ansatz with long-range AF orders has successfully reproduced the ground-state phase diagram from ED⁴ and DMRG⁵ calculations. The AF-fRVB wave function also captures a second-order transition at $J_2 = 0.45$ and a first-order transition at $J_2 = 0.6$ that is consistent with the conclusion made by the bosonic RVB states¹⁰. The AF-fRVB state naturally solves the problem that the purely fermionic RVB state cannot describe the magnetic ordered state for $J_2 < 0.45$ and $J_2 > 0.6$. We have shown that the AF-fRVB wave function with few variational parameters can reach almost the same energy as the PEPS with very large bond dimension. In addition, although the mean-field spinon spectrum is gapful for $d_{x^2-y^2} + d_{xy}$ symmetry, the degeneracy from s_{+-} and d_{xy} pairing symmetries in the frustrated regime suggests that the spin-liquid phase can also exhibit Dirac spinon spectrum as a result of $d+s$ pairing symmetry.

We would like to thank F. Yang and T. Ma for useful discussions. C.P.C. is supported by Chinese Academy of Engineering Physics and Ministry of Science and Technology. The calculations are performed in the National Center for High-performance Computing. H.Y.C. is supported by National Science Council of Taiwan under Grant No. NSC-101-2112-M-003-005-MY3 and National Center for Theoretical Science of Taiwan.

- ¹ L. Balents, Nat. Phys. **464**, 199 (2010).
- ² B. Normand, Contemp. Phys. **50**, 533 (2009).
- ³ M. Mambri, A. Lauchli, D. Poilblanc, and F. Mila, Phys. Rev. B **74**, 144422 (2006).
- ⁴ J. Richter and J. Schulenburg, Eur. Phys. J. B **73**, 117 (2010).
- ⁵ H.-C. Jiang, H. Yao, and L. Balents, Phys. Rev. B **86**, 024424 (2012).
- ⁶ S.-S. Gong *et al.*, arXiv:1311.5962 (2013).
- ⁷ L. Capriotti, F. Becca, A. Parola, and S. Sorella, Phys. Rev. Lett. **87**, 097201 (2001).
- ⁸ J. Lou and A. W. Sandvik, Phys. Rev. B **76**, 104432 (2007).
- ⁹ F. Mezzacapo, Phys. Rev. B **86**, 045115 (2012).
- ¹⁰ T. Li, F. Becca, W. Hu, and S. Sorella, Phys. Rev. B **86**, 075111 (2012).
- ¹¹ L. Wang, D. Poilblanc, Z. C. Gu, X. G. Wen, and F. Verstraete, Phys. Rev. Lett. **111**, 037202 (2013).
- ¹² W. J. Hu, F. Becca, A. Parola, and S. Sorella, Phys. Rev. B **88**, 060402(R) (2013).
- ¹³ Y. Qi and Z.-C. Gu, arXiv:1308.2759 (2013).
- ¹⁴ P. W. Anderson, Science **235**, 1196 (1987).
- ¹⁵ X.-G. Wen, Phys. Rev. B **65**, 165113 (2002).
- ¹⁶ A. Auerbach and D. P. Arovas, Phys. Rev. Lett. **61**, 617 (1988).
- ¹⁷ D. P. Arovas and A. Auerbach, Phys. Rev. B **38**, 316 (1988).
- ¹⁸ R. Flint and P. Coleman, Phys. Rev. B **79**, 014424 (2009).
- ¹⁹ S. Yunoki and S. Sorella, Phys. Rev. B **74**, 014408 (2006).
- ²⁰ Y. Ran, M. Hermele, P. A. Lee, and X.-G. Wen, Phys. Rev. Lett. **98**, 117205 (2007).
- ²¹ T. Li, arXiv:1101.1352 (2011).
- ²² L. Wang, Z.-C. Gu, F. Verstraete, and X.-G. Wen, arXiv:1112.3331 (2012).

- ²³ R. Darradi *et al.*, Phys. Rev. B **78**, 214415 (2008).
- ²⁴ L. Capriotti, F. Becca, A. Parola, and S. Sorella, Phys. Rev. B **67**, 212402 (2003).
- ²⁵ P. J. Hirschfeld, M. M. Korshunov, and I. I. Mazin, Rep. Prog. Phys. **74**, 124508 (2011).
- ²⁶ E. Dagotto and A. Moreo, Phys. Rev. Lett. **63**, 2148 (1989).
- ²⁷ H. J. Schulz, T. A. L. Ziman, and D. Poilblanc, J. Phys. I **6**, 675 (1996).
- ²⁸ J.-F. Yu and Y.-J. Kao, Phys. Rev. B **85**, 094407 (2012).
- ²⁹ D. J. Scalapino, Phys. Rep. **250**, 329 (1995).